Editors' Suggestion

Interface-Governed Deformation of Nanobubbles and Nanotents Formed by Two-Dimensional Materials

Zhaohe Dai,[1] Yuan Hou,[2] Daniel A. Sanchez,[3] Guorui Wang,[2] Christopher J. Brennan,[4] Zhong Zhang,[2] Luqi Liu,[2,*] and Nanshu Lu[1,3,4,5,†]

[1]*Center for Mechanics of Solids, Structures and Materials, Department of Aerospace Engineering and Engineering Mechanics, The University of Texas at Austin, Austin, Texas 78712, USA*

[2]*CAS Key Laboratory of Nanosystem and Hierarchical Fabrication, CAS Center for Excellence in Nanoscience National Center for Nanoscience and Technology, Beijing 100190, China*

[3]*Texas Materials Institute, The University of Texas at Austin, Austin, Texas 78712, USA*

[4]*Department of Electrical and Computer Engineering, The University of Texas at Austin, Austin, Texas 78712, USA*

[5]*Department of Biomedical Engineering, The University of Texas at Austin, Austin, Texas 78712, USA*

(Received 27 July 2018; published 26 December 2018)

Nanoblisters such as nanobubbles and nanotents formed by two-dimensional (2D) materials have been extensively exploited for strain engineering purposes as they can produce self-sustained, nonuniform in-plane strains through out-of-plane deformation. However, deterministic measure and control of strain fields in these systems are challenging because of the atomic thinness and unconventional interface behaviors of 2D materials. Here, we experimentally characterize a simple and unified power law for the profiles of a variety of nanobubbles and nanotents formed by 2D materials such as graphene and MoS_2 layers. Using membrane theory, we analytically unveil what sets the in-plane strains of these blisters regarding their shape and interface characteristics. Our analytical solutions are validated by Raman spectroscopy measured strain distributions in bulged graphene bubbles supported by strong and weak shear interfaces. We advocate that both the strain magnitudes and distributions can be tuned by 2D material-substrate interface adhesion and friction properties.

DOI: 10.1103/PhysRevLett.121.266101

Two-dimensional (2D) materials are atomically thin crystals with unique properties that lend well to next-generation ultrathin electronic and optoelectronic devices [1–4]. It has been well established that mechanical strain can strongly perturb the band structure of these materials, giving rise to the possibility of using mechanical deformation to tune their electronic and photonic performance dramatically [5–9]. In fact, this principle, termed strain engineering, is now routinely used in manufacturing traditional semiconductor devices [10]. The strain engineering of 2D materials is particularly exciting because an individual atomic sheet is intrinsically capable of sustaining much larger mechanical strain compared to either their bulk counterparts or conventional electronic materials [11,12]. Also, the atomic thickness of 2D materials allows them to be easily poked or pressurized from the third dimension (i.e., perpendicular to their plane of atoms) [13–17]. The resulting configurations including nanoscale bubbles and tents can be called by a unified name, 2D material blisters [13–20]. Recently, the considerable strain associated with these nanoblisters has created opportunities for the study of new fundamental physics and applications such as enormous pseudomagnetic fields, large-scale quantum emitters, and so on [21–23].

A major challenge in these systems is to find out or even control the strain in the blisters deterministically, calling for understanding and validating how the blister geometry intertwines with mechanics in these atomic sheets [24,25]. So far, self-similar profiles of the 2D material bubbles have been widely discovered in experiments [15,17,26,27]. However, it remains challenging to analytically relate the bubble and tent shape characteristics to the full-field strain distributions and experimentally prove the relation. Consequently, accurate strain tuning through blister shape adjustments is still elusive [21,22,24]. One difficulty comes from the intrinsically nonlinear coupling between in-plane strain and out-of-plane deformations predicted by the membrane theory [28]. More fundamental concern arises from the subtle nature of 2D materials, where the material thickness approaches the atomic scale and the surface is atomically smooth [29]. These features even challenge the applicability of continuum theories from a perspective of deformation physics [30–34]. As a result, the prevailing analysis of the strain distribution and strain-coupled physics and chemistry in 2D material blisters relies heavily on numerical techniques, such as case-by-case molecular dynamics (MD) simulations [22,24,35–37]. To deal with these concerns, a combination of continuum theories with microscale experiments is highly needed and yet to emerge so far.

Herein, we experimentally explore the strain field in nanoblisters formed by 2D materials accounting for

different natures of 2D materials interfaces. Using tapping mode atomic force microscopy (AFM), we experimentally characterized a variety of bubbles and tents formed by graphene and MoS_2 layers. Their shapes were empirically found to follow a simple power law, enabling closed-form analytical solutions to the Föppl–von Kármán equations at the membrane limit. Our results show that the strain distribution in the 2D material can be estimated by simply measuring the height and radius of the bubbles and tents, and that the strain highly depends on the interfacial interaction between the 2D material and the underlying substrate. To validate our analytical solutions, we experimentally carried out Raman mapping on pressurized graphene nanobubbles with strong (graphene-SiO_2) and weak (graphene-graphene) shear interfaces. The measured and analytically predicted Raman shifts have found good matches for both types of interfaces.

We first investigate the shape characteristics of both nanobubbles and nanotents of 2D materials, which can form spontaneously or be created in a controllable manner. For the spontaneous case, nanometer-scale bubbles and tents form when monolayer or few-layer 2D materials are exfoliated or transferred on a target substrate. The formation mechanism is typically attributed to the inevitably trapped water, hydrocarbon, and/or nanoparticles at the 2D material-substrate interface during sample preparation [15,17]. The spontaneously formed nanobubbles and nanotents analyzed in this study were made by mechanically exfoliating few- and monolayer graphene and MoS_2 from their bulk crystals on silicon substrate, or transferring CVD-grown MoS_2 on a gold or Al_2O_3 substrate [38]. Details on the transfer process for different types of samples are provided in the methods section of the Supplemental Material [39]. Figure 1(a) displays typical examples of nanobubbles formed by monolayer graphene on SiO_2. When nanoparticles were trapped, 2D materials can drape around the nanoparticle, forming micro- or nanotents as shown in Figs. 1(b) and 1(c). To form controllable bubbles, we transferred monolayer graphene and a 4-layer MoS_2 to cover prepatterned microcavities in SiO_2 to form suspended drumheads and then followed a well-established gas diffusion procedure to bulge the drumheads [16]. In this case, the bubbles can be pressurized controllably [Fig. 1(d) [39]].

The out-of-plane profiles of all the different types of bubbles and tents prepared by us and collected from the literature are summarized in Fig. 2. Although the radii of the 2D material blisters range from tens to thousands of nanometers, we realized that the height profiles of bubbles and tents collapse onto two master curves if we normalize the out-of-plane deflection (w) of each blister by its central height (h), and the radial positions (r) by its radius (a). We discovered that the collapsed height profiles can be described by a unified power form,

$$\frac{w}{h} = 1 - \left(\frac{r}{a}\right)^{\alpha}, \tag{1}$$

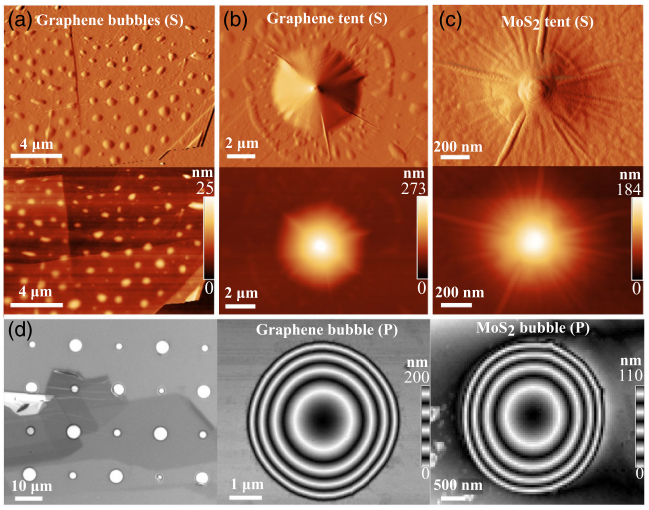

FIG. 1. From top to bottom: Atomic force microscopy (AFM) phase and height images of spontaneously formed graphene bubbles on SiO_2 (a), a multilayer graphene tent on SiO_2 (b), and a CVD-MoS_2 tent on gold film (c). (d) From left to right: optical image of graphene flakes exfoliated on prepatterned SiO_2 with microcavities, AFM height images of a monolayer graphene bubble, and a four-layer MoS_2 bubble. Note that (S) represents bubbles or tents formed spontaneously while (P) represents those formed by controllable air pressurization.

where α is 2 for bubbles or 2/3 for tents. Note that Fig. 2 summarizes graphene and MoS_2 bubbles and tents with aspect ratios ranging from 0.05 to 0.20. Remarkably, regardless of the aspect ratios, the types of 2D material, the supporting substrates (silicon, alumina, or atomically flat 2D material flakes), the content in the bubble (liquid or gas), or the fabrication methods, all bubble profiles can collapse to Eq. (1) with $\alpha = 2$ [Fig. 2(a)]. We also found that for profiles of graphene and MoS_2 tents, data obtained from MD simulations or coarse-grained (CG) modeling [22,24,36] can also collapse to Eq. (1) with $\alpha = 2/3$ [Fig. 2(b)]. In fact, the empirical conclusion of $\alpha = 2$ is

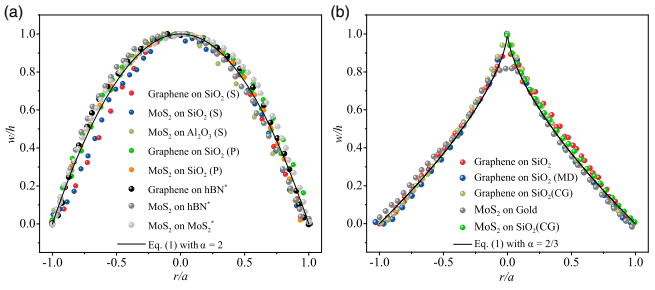

FIG. 2. Universal shape characteristics of 2D material bubbles and tents. (a) Normalized bubble profiles measured by our experiments and collected from literature. Note that samples from Ref. [17] feature atomically smooth interfaces, are labeled by *. (b) Normalized tent profiles measured by our experiments and simulation results in the literature. The simulation data about graphene and MoS_2 is from Refs. [36,24], respectively.

a widely adopted simple membrane solution for blisters [48,49] and $\alpha = 2/3$ is well matched with the analytical solution to an indented blister in the literature [28,50]. We thus conclude that this simple power form can be a good approximation for describing the profiles of 2D material bubbles and tents.

Now that the out-of-plane displacement of 2D material blisters is readily available as given in Eq. (1), we can try to solve the in-plane displacement and then calculate strains out of displacements. Attributing to the atomic thinness of 2D materials, it is sufficient to simply use the membrane limit of the Föppl–von Kármán equations [28,48]. The in-plane equilibrium equation in terms of displacements is therefore

$$\frac{d^2u}{dr^2} + \frac{1}{r}\frac{du}{dr} - \frac{u}{r^2} = -\frac{1-\nu}{2r}\left(\frac{dw}{dr}\right)^2 - \frac{dw}{dr}\frac{d^2w}{dr^2}, \quad (2)$$

where u is the in-plane displacement of the 2D material and ν is the Poisson's ratio. Plugging Eq. (1) into this equation and solving the 2nd order ODE using the finite condition when $r \to 0$ can yield an analytical solution to the in-plane displacement:

$$u = \zeta(\nu)\frac{h^2}{a}\left[\frac{r}{a} - \left(\frac{r}{a}\right)^{2\alpha-1}\right] + u_s\frac{r}{a}, \quad (3)$$

where $\zeta(\nu) = \{[\alpha(2\alpha - 1 - \nu)]/[8(\alpha - 1)]\}$ and u_s is a constant related to the slippage at the edge of the blister ($r = a$). This explicit displacement field allows for the direct solutions for both the radial and circumferential strain fields:

$$\varepsilon_r = \begin{cases} \zeta(\nu)\frac{h^2}{a^2}\left[1 - \frac{1+\nu-2\alpha\nu}{2\alpha-1-\nu}\left(\frac{r}{a}\right)^{2\alpha-2}\right] + \frac{u_s}{a}, & r \le a \\ -\frac{au_s}{r^2}, & r > a \end{cases}, \quad (4a)$$

$$\varepsilon_\theta = \begin{cases} \zeta(\nu)\frac{h^2}{a^2}\left[1 - \left(\frac{r}{a}\right)^{2\alpha-2}\right] + \frac{u_s}{a}, & r \le a \\ \frac{au_s}{r^2}, & r > a \end{cases}. \quad (4b)$$

Clearly, the sliding of the 2D material-substrate interface ($u_s \neq 0$) can induce nonzero strain in the supported zone ($r > a$), which is important for strain engineering applications of 2D materials [35]. Typically, the edge of the 2D material blister is assumed to be fully clamped due to adhesion and strong shear interactions with the supporting substrate outside of boundary [11,22.16]. However, the atomically smooth surfaces of 2D materials make interfacial sliding particularly easy. Recent experiments on gas-pressurized graphene bubbles revealed that the shear interactions between graphene and its substrate can be fairly weak, leading to nonlinear, deflection-dependent interface sliding displacements [14,51]. It has also been discovered that well-established theories assuming clamped conditions offer good approximations only when the deflection is small ($h/a < 0.1$), while experimental measurements deviated from theories with clamped boundaries in samples with large deflection [14]. Recent studies on 2D material interface further highlighted the so-called superlubrication (near-zero friction) when a 2D material sits on atomically smooth substrates, including itself, which is very common in 2D materials devices [52].

Considering that the graphene and MoS_2 blisters in Fig. 2 encompass either relatively strong interfaces with small deflections or atomically lubricated interfaces, our prime interest of this study is in two limits: strong-shear limit (clamped, fully bonded interface) and weak-shear limit (sliding, frictionless interface). For the former, we can apply clamped boundary at the edge of the blister. For the latter, the stress and displacement in the outer supported region can be obtained as the classical Lamé problem in linear elasticity [53]. The stress and displacement continuity then leads to [39]

$$u_s = \begin{cases} 0, & \text{strong-shear limit} \\ -\frac{\alpha(1+\nu)}{8}\frac{h^2}{a}, & \text{weak-shear limit} \end{cases}. \quad (5)$$

Now Eqs. (4) and (5) combined offer the complete analytical solutions to the strain field in 2D materials forming blisters, with either strong or weak interaction with their substrates. After appropriately choosing the α and u_s according to the specific blister shape and 2D material-substrate interface, one can easily compute the strain distribution inside and outside of a 2D blister by simply measuring its height and radius. We note that a generalized analysis may be performed by accounting for the detailed frictional resistance (e.g., the stick-slip behavior) at the 2D material-substrate interface [54].

In Fig. 3, we plot the strain distributions of the 2D material blister as solid curves using our equations. The strain is normalized by h^2/a^2 such that the distribution will only depend on the interface conditions and material

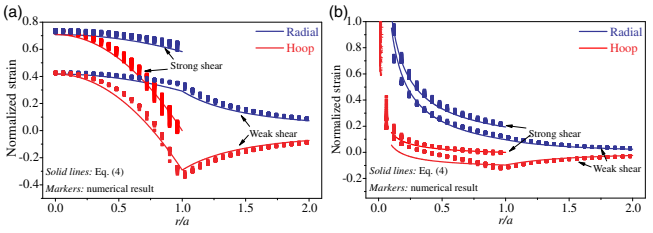

FIG. 3. Normalized strain distribution curves predicted by our analytical solution (solid lines) and solved by numerical analysis (markers) in bubbles (a) and tents (b), subjected to both clamped (strong interface) and frictionless (sliding interfaces) boundary conditions. The strain is normalized by h^2/a^2, giving rise to deflection-independent curves. The numerical results are solved for a monolayer graphene with aspect ratios ranging from $0.02 < h/a < 0.2$.

properties, i.e., the Poisson's ratio. Comparing Fig. 3(a) for bubbles and Fig. 3(b) for tents, it is clear that the strain gradients are much larger in tents, with strain divergence towards the center of the tents due to the assumed point load. Note that under the same aspect ratio, interface sliding can considerably reduce the strain level in 2D material blisters in comparison with blisters with strong-shear interfaces. This highlights the importance of accounting for the ultralubricated interface in the case that the 2D material is supported by an atomically smooth substrate.

Next, we try to verify our analytical solutions numerically. We solved the nonlinear Föppl–von Kármán equations with clamped and slipping boundaries, where the bending behavior is also considered for generality [39]. The numerical solutions are plotted as markers in Fig. 3 for monolayer graphene with aspect ratios ranging from 0.05 to 0.20, to directly compare with the analytical solutions (solid curves). Since analytically solved strains are strictly proportional to h^2/a^2, after normalization, the solid curves are no longer dependent on the aspect ratio. However, the numerically solved strains show more complicated dependence on the aspect ratio, because the markers for different aspect ratios do not fully collapse. Despite this small discrepancy, the overall good agreement between the two solutions indicates that for our experimentally observed blisters with aspect ratios ranging from 0.05 to 0.20, bending effects are negligible. Thus, the numerical results have verified that our analytical solution given by Eq. (4) is a reasonable estimation for strains in both bubbles and tents under both clamped and slipping boundary conditions.

Our analytical solution, though verified numerically, is still challenged by a widespread concern on the breakdown of classical membrane theories at the atomic limit [30–34]. To examine the applicability of our analytical solutions, we performed graphene bulging experiments with intentionally designed strong- and weak-shear interfaces. Monolayer graphene sealed microcavities were fabricated by micromechanical cleavage of graphene over SiO_2 substrate with prepatterned 2.5-micron-radius holes [Fig. 4(a)]. Following a well-developed gas diffusion method [16], we can create a pressure difference across the monolayer and bulge it in a controlled manner.

The strong-shear-interface graphene bubble was generated by pressurizing a graphene monolayer on SiO_2 with the maximum deflection less than 150 nm. Under this condition, the interface sliding was found to be minimal; thus it is compatible with the clamped interface assumption [14]. To experimentally study the weak-shear case, we assembled a graphene-SiO_2 supporting substrate for the graphene bubble [Fig. 4(b)]. First, few-layer graphene was transferred over a SiO_2 microhole. The suspended portion of the multilayer graphene was then etched to open up the microhole. After creating an atomically flat region around the microhole, a monolayer graphene was precisely transferred to cover this microhole, resulting in a graphene

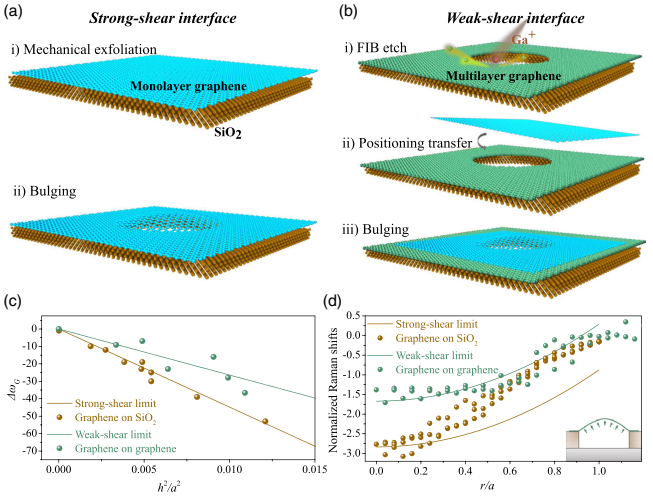

FIG. 4. Schematics of the graphene drumheads formed on a SiO_2 substrate (a) and on a graphene-covered SiO_2 substrate (b). (c) Raman shifts of the G band at the center of graphene bubbles predicted by our analytical solution (solid curves) and measured by our experiments (markers). (d) Normalized Raman shifts of the G band ($\Delta\omega_G a^2/\omega_0 h^2$) as functions of the normalized radial position (r/a) for monolayer graphene bubbles.

drumhead supported by few-layer graphene [39]. Applying a differential pressure across the suspended graphene membrane, this graphene bubble was expected to bulge under weak-shear interface as the graphene-graphene interface can be considered as superlubricated.

We performed multiple AFM and Raman characterizations on the graphene bubbles with well-controlled interfaces [39]. For an axisymmetric graphene bubble, the G band shifts in the Raman spectrum are related to the strain components through the following equation [55]:

$$\frac{\Delta\omega_G}{\omega_0} = -\gamma(\varepsilon_r + \varepsilon_\theta) \pm \frac{\beta}{2}(\varepsilon_r - \varepsilon_\theta), \tag{6}$$

where ε_r and ε_θ are analytically expressed in Eq. (4), γ is the Grüneisen parameter, and β is the shear deformation potential that details the amount of splitting in the G bands, which were experimentally calibrated for monolayer graphene ($\gamma = 1.99$ and $\beta = 0.99$) [56]. Therefore, analytical prediction for strain fields can be readily converted to analytical prediction for the G band shifts using Eq. (6). Particularly, at the center of the bubble where $\varepsilon_r = \varepsilon_\theta$, the G band shifts are predicted by Eqs. (4) and (6) to take a very simple form:

$$\Delta\omega_G = -c\gamma\omega_0 \frac{h^2}{a^2} \tag{7}$$

where the constant c is $[(3-\nu)/2]$ for bubbles supported by strong shear interfaces and is $(1-\nu)$ by weak shear interfaces.

Because of space limitations, we present the details of the experimental Raman characterizations in the Supplemental Material, Note 2 [39]. Here, we first show the

Raman G band shifts at the center of graphene bubbles as a function of h^2/a^2 in Fig. 4(c), which is predicted to be linear by our analytical solution in Eq. (8). The markers represent experimental data for both SiO_2- (brown) and graphene-supported (green) graphene bubbles and the solid curves correspond to predicted G band shifts for strong- (green) and weak-shear-interfaced (brown) 2D material bubbles. By setting the Poisson's ratio of graphene to be 0.165 in Eq. (7), we find good agreement between our theoretical predictions and experimental measurements. This may confirm the applicability of our simplified membrane theory in relating the out-of-plane deformations to in-plane strains for 2D material blisters.

In Fig. 4(d), we further normalize both the measured and predicted G band shifts by h^2/a^2 and plot them as functions of the normalized radial position r/a. Our weak-shear and strong-shear model can partially capture the full-field strain distribution in graphene-on-graphene and graphene-on-SiO_2 bubbles, respectively. However, deviation between predicted and measured G band shifts occurs and enlarges towards the edge of the bubble, especially for SiO_2-supported graphene bubbles. We attribute such edge deviation in Fig. 4(d) to the limited spatial resolution of Raman spectroscopy ($\sim 1\ \mu$m) and the possible doping effect by the substrate [57,58], which are further elucidated in Figs. S9 and S10 [39]. As for 2D material tents, a recent study reported the Raman 2D band shifts for a SiN/Si-supported graphene drumhead subjected to nanoindentation [59]. The experimental results can be well captured by our analytical solution to a 2D material tent with strong-shear interface (Fig. S11 [39]). We thus claim that our analytical solutions in Eq. (5), enabled by the shape characteristics in Fig. 2, can offer valid estimation for the in-plane strain in 2D material bubbles and tents simply by knowing their height and radius. It is especially true at the center of bubbles by Eq. (7), which may, in turn, be used to measure the Grüneisen parameter for the broadly extended 2D material family.

The 2D material bubble and tent structures have been exploited in many recent studies [17–22,27,60–64] where people typically use prepatterned micropillars or interface-confined contents to produce a single or an array of 2D material blisters. Our findings show that the strain in blisters highly hinges on their aspect ratio (h/a). We note that a balance between adhesion (which favors large areas of contact) and stretching energy (which diminishes in blisters of large radius) dictates a constant aspect ratio:

$$h/a = (\phi \Delta\gamma / E_{2D})^{1/4}. \tag{8}$$

where $\Delta\gamma$ is energy change per unit area, E_{2D} is the in-plane stiffness of the 2D material, and ϕ is a constant prefactor. Equation (8) implies that the aspect ratio or ultimately the strain of a 2D material bubble or tent is dominated by the ratio of the 2D material-substrate adhesion to the in-plane stiffness of the 2D material. In fact, this interface- and stiffness-dependent out-of-plane deformation characteristic has been observed at a variety of length scales—from graphene to polymer films with thicknesses ranging from 1 nm to 1 mm [50]. Here, we determine ϕ for 2D material bubbles and tents of both strong- and weak-shear interfaces in Table I [39]. Notably, recent experimental discovery of the constant aspect ratio of 2D material bubbles for a given 2D material-substrate system provided a good validation [17], and there is no available experimental data for 2D material tents so far.

TABLE I. The prefactor ϕ that determines the aspect ratio by $\Delta\gamma/E_{2D}$ in Eq. (8).

Shape		Strong shear	Weak shear
Bubble	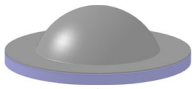	$\{[24(1-\nu)]/[5(7-\nu)]\}$	(6/5)
Tent	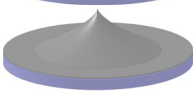	$\{[72(1-\nu)]/[5-3\nu]\}$	18

This work is supported by the NSF Division of Civil, Mechanical and Manufacturing Innovation (CMMI) under Grant No. 1351875, the CNS Catalyst Grant at the University of Texas at Austin, and the National Natural Science Foundation of China (Grant No. 21474023). Z. D. acknowledges Dr. Peng Wang and Professor Rui Huang (UT Austin) for their assistance in numerical method.

*To whom all correspondence should be addressed.
liulq@nanoctr.cn
†To whom all correspondence should be addressed.
nanshulu@utexas.edu

[1] R. Mas-Balleste, C. Gomez-Navarro, J. Gomez-Herrero, and F. Zamora, Nanoscale **3**, 20 (2011).
[2] K. S. Novoselov, A. Mishchenko, A. Carvalho, and A. H. Castro Neto, Science **353**, aac9439 (2016).
[3] D. Akinwande, N. Petrone, and J. Hone, Nat. Commun. **5**, 5678 (2014).
[4] C. Choi *et al.*, Nat. Commun. **8**, 1664 (2017).
[5] D. Lloyd, X. Liu, J. W. Christopher, L. Cantley, A. Wadehra, B. L. Kim, B. B. Goldberg, A. K. Swan, and J. S. Bunch, Nano Lett. **16**, 5836 (2016).
[6] A. Branny, S. Kumar, R. Proux, and B. D. Gerardot, Nat. Commun. **8**, 15053 (2017).
[7] H. Li *et al.*, Nat. Commun. **6**, 7381 (2015).
[8] G. G. Naumis, S. Barraza-Lopez, M. Oliva-Leyva, and H. Terrones, Rep. Prog. Phys. **80**, 096501 (2017).
[9] G. da Cunha Rodrigues, P. Zelenovskiy, K. Romanyuk, S. Luchkin, Y. Kopelevich, and A. Kholkin, Nat. Commun. **6**, 7572 (2015).
[10] J. A. Del Alamo, Nature (London) **479**, 317 (2011).
[11] C. Lee, X. Wei, J. W. Kysar, and J. Hone, Science **321**, 385 (2008).

[12] C. Androulidakis, K. Zhang, M. Robertson, and S. H. Tawfick, 2D Mater. **5**, 032005 (2018).
[13] D. Davidovikj, F. Alijani, S. Cartamil-Bueno, H. Zant, M. Amabili, and P. Steeneken, Nat. Commun. **8**, 1253 (2017).
[14] G. Wang, Z. Dai, Y. Wang, P. H. Tan, L. Liu, Z. Xu, Y. Wei, R. Huang, and Z. Zhang, Phys. Rev. Lett. **119**, 036101 (2017).
[15] D. A. Sanchez, Z. Dai, P. Wang, A. Cantu-Chavez, C. J. Brennan, R. Huang, and N. Lu, Proc. Natl. Acad. Sci. U.S.A. **115**, 7884 (2018).
[16] S. P. Koenig, N. G. Boddeti, M. L. Dunn, and J. S. Bunch, Nat. Nanotechnol. **6**, 543 (2011).
[17] E. Khestanova, F. Guinea, L. Fumagalli, A. K. Geim, and I. V. Grigorieva, Nat. Commun. **7**, 12587 (2016).
[18] A. Reserbat-Plantey *et al.*, Nano Lett. **14**, 5044 (2014).
[19] H. Tomori, A. Kanda, H. Goto, Y. Ootuka, K. Tsukagoshi, S. Moriyama, E. Watanabe, and D. Tsuya, Appl. Phys. Express **4**, 075102 (2011).
[20] J. M. Lee *et al.*, Nano Lett. **10**, 2783 (2010).
[21] N. Levy, S. Burke, K. Meaker, M. Panlasigui, A. Zettl, F. Guinea, A. C. Neto, and M. Crommie, Science **329**, 544 (2010).
[22] N. N. Klimov, S. Jung, S. Zhu, T. Li, C. A. Wright, S. D. Solares, D. B. Newell, N. B. Zhitenev, and J. A. Stroscio, Science **336**, 1557 (2012).
[23] C. Palacios-Berraquero, D. M. Kara, A. R.-P. Montblanch, M. Barbone, P. Latawiec, D. Yoon, A. K. Ott, M. Loncar, A. C. Ferrari, and M. Atatüre, Nat. Commun. **8**, 15093 (2017).
[24] J. Feng, X. Qian, C.-W. Huang, and J. Li, Nat. Photonics **6**, 866 (2012).
[25] D. Vella and B. Davidovitch, Soft Matter **13**, 2264 (2017).
[26] G. Zamborlini, M. Imam, L. L. Patera, T. O. Menteş, N. Stojić, C. Africh, A. Sala, N. Binggeli, G. Comelli, and A. Locatelli, Nano Lett. **15**, 6162 (2015).
[27] H. Ghorbanfekr-Kalashami, K. S. Vasu, R. R. Nair, F. M. Peeters, and M. Neek-Amal, Nat. Commun. **8**, 15844 (2017).
[28] E. H. Mansfield, *The Bending and Stretching of Plates* (Cambridge University Press, Cambridge, England, 2005).
[29] X. Li, L. Tao, Z. Chen, H. Fang, X. Li, X. Wang, J.-B. Xu, and H. Zhu, Appl. Phys. Rev. **4**, 021306 (2017).
[30] G. López-Polín, C. Gómez-Navarro, V. Parente, F. Guinea, M. I. Katsnelson, F. Pérez-Murano, and J. Gómez-Herrero, Nat. Phys. **11**, 26 (2015).
[31] L. Tapasztó, T. Dumitrică, S. J. Kim, P. Nemes-Incze, C. Hwang, and L. P. Biró, Nat. Phys. **8**, 739 (2012).
[32] J. H. Los, A. Fasolino, and M. I. Katsnelson, Phys. Rev. Lett. **116**, 015901 (2016).
[33] R. J. T. Nicholl, N. V. Lavrik, I. Vlassiouk, B. R. Srijanto, and K. I. Bolotin, Phys. Rev. Lett. **118**, 266101 (2017).
[34] D.-B. Zhang, E. Akatyeva, and T. Dumitrică, Phys. Rev. Lett. **106**, 255503 (2011).
[35] Z. Qi, A. L. Kitt, H. S. Park, V. M. Pereira, D. K. Campbell, and A. H. Castro Neto, Phys. Rev. B **90**, 125419 (2014).
[36] S. Zhu, Y. Huang, N. N. Klimov, D. B. Newell, N. B. Zhitenev, J. A. Stroscio, S. D. Solares, and T. Li, Phys. Rev. B **90**, 075426 (2014).
[37] Z. Meng, R. A. Soler-Crespo, W. Xia, W. Gao, L. Ruiz, H. D. Espinosa, and S. Keten, Carbon **117**, 476 (2017).
[38] Y. Huang, E. Sutter, N. N. Shi, J. Zheng, T. Yang, D. Englund, H. J. Gao, and P. Sutter, ACS Nano **9**, 10612 (2015).
[39] See Supplemental Material at http://link.aps.org/supplemental/10.1103/PhysRevLett.121.266101 for material preparations, experimental setup, and characterizations, and analysis based on membrane mechanics, which includes Refs. [40–47].
[40] C. J. Brennan, R. Ghosh, K. Koul, S. K. Banerjee, N. Lu, and E. T. Yu, Nano Lett. **17**, 5464 (2017).
[41] R. Frisenda, E. Navarro-Moratalla, P. Gant, D. Perez De Lara, P. Jarillo-Herrero, R. V. Gorbachev, and A. Castellanos-Gomez, Chem. Soc. Rev. **47**, 53 (2018).
[42] Y. Zhang, C. Hui, R. Sun, K. Li, K. He, X. Ma, and F. Liu, Nanotechnology **25**, 135301 (2014).
[43] L. G. Cancado, A. Jorio, E. H. Martins Ferreira, F. Stavale, C. A. Achete, R. B. Capaz, M. V. O. Moutinho, A. Lombardo, T. S. Kulmala, and A. C. Ferrari, Nano Lett. **11**, 3190 (2011).
[44] A. C. Ferrari, Solid State Commun. **143**, 47 (2007).
[45] C. Metzger, S. Rémi, M. Liu, S. V. Kusminskiy, A. H. Castro Neto, A. K. Swan, and B. B. Goldberg, Nano Lett. **10**, 6 (2010).
[46] Z. H. Ni, T. Yu, Y. H. Lu, Y. Y. Wang, Y. P. Feng, and Z. X. Shen, ACS Nano **2**, 2301 (2008).
[47] K. M. Yue, W. Gao, R. Huang, and K. M. Liechti, J. Appl. Phys. **112**, 083512 (2012).
[48] L. B. Freund and S. Suresh, *Thin Film Materials: Stress, Defect Formation and Surface Evolution* (Cambridge University Press, Cambridge, England, 2004).
[49] P. Wang, W. Gao, Z. Cao, K. M. Liechti, and R. Huang, J. Appl. Mech. **80**, 040905 (2013).
[50] J. Chopin, D. Vella, and A. Boudaoud, Proc. R. Soc. A **464**, 2887 (2008).
[51] A. L. Kitt, Z. Qi, S. Rémi, H. S. Park, A. K. Swan, and B. B. Goldberg, Nano Lett. **13**, 2605 (2013).
[52] O. Hod, M. Urbakh, D. Naveh, M. Bar-Sadan, and A. Ismach, Adv. Mater. **30**, 1706581 (2018).
[53] M. H. Sadd, *Elasticity: Theory, Applications, and Numerics* (Academic Press, Burlington, MA, 2009).
[54] Q. Li, C. Lee, R. W. Carpick, and J. Hone, Phys. Status Solidi B **247**, 2909 (2010).
[55] M. Huang, H. Yan, C. Chen, D. Song, T. F. Heinz, and J. Hone, Proc. Natl. Acad. Sci. U.S.A. **106**, 7304 (2009).
[56] T. M. G. Mohiuddin,, A. Lombardo, R. R. Nair, A. Bonetti, G. Savini, R. Jalil, N. Bonini, D. M. Basko, C. Galiotis, N. Marzari, K. S. Novoselov, A. K. Geim, and A. C. Ferrari, Phys. Rev. B **79**, 205433 (2009).
[57] J. E. Lee, G. Ahn, J. Shim, Y. S. Lee, and S. Ryu, Nat. Commun. **3**, 1024 (2012).
[58] A. Das *et al.*, Nat. Nanotechnol. **3**, 210 (2008).
[59] K. Elibol, B. C. Bayer, S. Hummel, J. Kotakoski, G. Argentero, and J. C. Meyer, Sci. Rep. **6**, 28485 (2016).
[60] K. Xu, P. Cao, and J. R. Heath, Science **329**, 1188 (2010).
[61] K. Vasu *et al.*, Nat. Commun. **7**, 12168 (2016).
[62] Z. Chen *et al.*, Nat. Commun. **8**, 14548 (2017).
[63] Y. Jiang, J. Mao, J. Duan, X. Lai, K. Watanabe, T. Taniguchi, and E. Y. Andrei, Nano Lett. **17**, 2839 (2017).
[64] D. Akinwande *et al.*, Extreme Mech. Lett. **13**, 42 (2017).